

# Structural Study of Ordering in the Normal-Commensurate Transition of $\{\text{N}(\text{CH}_3)_4\}_2\text{MnCl}_4$ --- Models and Adaptation ---

Naohiro KOSHIJI\*<sup>1</sup> and Hiroyuki MASHIYAMA

*Faculty of Science, Yamaguchi University, Yamaguchi 753-8512, Japan*

*<sup>1</sup>Kurume National College of Technology, Kurume 830-8555, Japan*

(Received September 18, 2010; accepted April 4, 2011)

The ordering process of constituent molecules in phase III of  $\{\text{N}(\text{CH}_3)_4\}_2\text{MnCl}_4$  is discussed on the basis of the results of X-ray structural analyses performed at nine temperatures below the normal-commensurate transition point. The order-disorder and displacive models are analyzed and compared in terms of the temperature dependences of structural parameters. Consequently, it is concluded that both tetramethylammonium and tetrachloromanganese ions behave as order-disorder units, and that their occupation probability, representative of the order parameter, changes monotonically with decreasing temperature. The results of our detailed analysis indicate that the centers of mass of the tetrahedral molecules shift continuously together with occupation ordering. The temperature dependence of the atomic displacement parameters is also investigated to confirm that the transition is of the order-disorder type.

KEYWORDS: commensurate phase, structure analysis, split atom method, occupation probability, structural phase transition

---

\* E-mail: koshi@kurume-nct.ac.jp

## 1. Introduction

In the course of systematic searches for novel ferroelectric materials, Sawada *et al.* found ferroelectricity in  $\{\text{N}(\text{CH}_3)_4\}_2\text{MCl}_4$  ( $M = \text{Zn}, \text{Co}$ ),<sup>1,2)</sup> which were at first considered to be similar to the incommensurate crystal of  $\text{K}_2\text{SeO}_4$ .<sup>3)</sup> Hereafter, we abbreviate  $\{\text{N}(\text{CH}_3)_4\}_2\text{MCl}_4$  to TMATC- $M$ , where TMA and TC- $M$  mean tetramethylammonium ion and tetrachlorometallic ion, respectively. Sawada *et al.* also investigated related crystals with  $M = \text{Fe}, \text{Ni}, \text{Cu}$  and  $\text{Mn}$ ; these crystals seemed to undergo successive transitions similarly to  $\text{Zn}$  and  $\text{Co}$  compounds. Soon after, ferroelectricity in TMATC- $\text{Fe}$  under hydrostatic pressure was reported, and the similarity of the pressure-temperature phase diagrams of different metallic ion compounds was recognized experimentally.<sup>4-6)</sup>

At room temperature or higher, the above compounds take a common orthorhombic structure with the space group  $Pm\bar{c}n$  ( $Z = 4$ ). This normal phase I transforms into the incommensurate phase II, which is followed by a commensurate phase III. Note that TMATC- $M$  ( $M = \text{Co}, \text{Zn}, \text{Fe}, \text{Mn}$ ) can be located on the universal  $p$ - $T$  phase diagram in the order of the  $M$ -Cl bond length; as the bond length increases, the pressure axis shifts to the lower side.<sup>6)</sup> The Mn-Cl bond length is largest among these four compounds, so TMATC-Mn can be located at the lowest end in the universal  $p$ - $T$  phase diagram.

A schematic phase diagram of TMATC-Mn is shown in Fig. 1.<sup>6-8)</sup> The incommensurate phase II may appear in a narrow temperature range between phases I and III at atmospheric pressure depending on the type of crystal. The commensurate phases III and IV take two- and three-fold cell length along the  $c$ -axis of the normal phase I. The transition temperatures are  $T_{\text{I-III}} = 293$  K,  $T_{\text{III-IV}} = 267$  K, and  $T_{\text{IV-V}} = 172$  K at atmospheric pressure, where phase II is omitted. The ferroelectric phase with a five-fold cell length appears only under high pressure. A number of commensurate phases have been recognized within the region of the incommensurate phase II.<sup>9, 10)</sup>

Fig. 1

The normal phase I of  $Pm\bar{c}n$  is common in many  $\text{A}_2\text{BX}_4$ -type ferroelectrics, and is considered as a prototype of successive transitions. Among  $\text{A}_2\text{BX}_4$ -type crystals,  $\text{K}_2\text{SeO}_4$  is well known for being of the displacive type in the normal-incommensurate transition; an optical phonon branch becomes soft at a wave number  $q_z = (1/3-\delta)$ , and the lock-in of the modulated wave number at  $q_z = 1/3$  induces ferroelectricity.<sup>3)</sup> On the other hand, many other  $\text{A}_2\text{BX}_4$ -type crystals do not manifest such a displacive nature, and the development of quasi-elastic or diffuse scattering around the normal-incommensurate transition suggests that the transition is of the order-disorder type.<sup>8)</sup> Note that the superlattice reflection intensity increases continuously with a similar power index, irrespective of the dynamic character of

the transition, whether it is of the order-disorder or displacive type.<sup>11, 12)</sup>

The relative ratio of the A ion size to the BX<sub>4</sub> tetrahedron size is empirically a characteristic measure of the normal-incommensurate transition in A<sub>2</sub>BX<sub>4</sub>-type compounds. When the ratio is large as in K<sub>2</sub>SeO<sub>4</sub>, BX<sub>4</sub> tetrahedrons can oscillate within the hexagonal network constructed by A ions. On the other hand, if the ratio is small as in Rb<sub>2</sub>ZnBr<sub>4</sub>, then the sterical exclusion effect prevents the displacive motion of BX<sub>4</sub> tetrahedrons, and the transition character would be of the order-disorder type. Such a simplified picture can explain why the soft phonon mode is observable only in K<sub>2</sub>SeO<sub>4</sub>.<sup>13)</sup>

In TMATC-*M*, A ions correspond to TMAs, which are not spherical but tetrahedral even if hydrogen atoms are neglected. NMR measurements indicate the highly mobile hydrogen atoms at room temperature.<sup>14)</sup> Although the situation may be more complicated, the universal *p*-*T* phase diagram for a number of TMATC-*M* compounds suggests that the physical size effect is important.

Concerning the phase transitions of TMATC-*M* compounds, we performed X-ray scattering experiments and investigated structural transformation through such phase transitions.<sup>15-19)</sup> In TMATC-Mn, we determined the crystal structure of phases I, III, IV and V, and discussed how constituent ions are modulated in commensurate phases.<sup>19)</sup> Furthermore, in our previous study,<sup>20)</sup> the crystal structure of the normal phase I was investigated in detail, especially near *T*<sub>I-III</sub>. We analyzed the structures of the normal phase by applying the disordered (OD) and displacive (DP) models. For the significant test on the *R* factor, the disordered model seemed to be more adequate than the displacive one. In the Fourier synthesis map of electron density, the disorderness of the TMA tetrahedron was demonstrated by typical double peaks. On the other hand, the electron density of Cl atoms constructing a MnCl<sub>4</sub> (abbreviated as TCM hereafter) tetrahedron had a regular elongated ellipsoid, and the set of atomic positions of Cl atoms estimated using the disordered model is arranged within a single-peak electron density map. It is still not conclusive whether the TCM tetrahedron is a disordered or displacive unit.

Following the concept of the split atom method, here let us give a rough sketch of a static character of the order-disorder behavior in Fig. 2. If an atom occupies two sites with equal probability  $p=1/2$ , then the distribution  $P(x)$  may be represented by the superposition  $P_1 + P_2$ , where  $P_1$  and  $P_2$  are single peak distributions at  $x = \pm d$ , with a variance  $\sigma$ . If  $d \geq \sqrt{\sigma}$ , then the superposed distribution will have two peaks, as in the case of TMA in phase I.

Fig. 2

However, the superposed distribution will be a single peak shape, if  $d < \sqrt{\sigma}$ . Such

distribution can be fitted by a wide distribution around the mean position, as shown by open circles denoted by PG in Fig. 2(a); this is an equivalent displacive distribution of the atom. The difference between the disordered and displacive distributions is small. We consider this to be the reason why the Cl atoms of  $\text{MnCl}_4$  were represented either by the disordered or displacive model successfully in the normal phase I.

When the mirror symmetry is broken in the ordered phase, the atomic distributions will change, as shown in Fig. 2(b). The solid curve and open circles show the order-disorder and displacive cases, respectively. If the difference between the two cases becomes larger, we will be able to distinguish between the two cases at lower temperatures, where  $d \geq \sqrt{\sigma}$ .

In this paper, we refine the crystal structure of the commensurate phase III by applying both disordered and displacive models, and investigate how the structure changes with decreasing temperature in phase III. In next section, the experimental details of the X-ray measurements and the procedure for reducing and analyzing intensity data are given. The commensurate structure and the structural change from the normal phase are described in the following section. In the final section, the temperature dependences of the order parameter and the atomic displacement parameters are discussed by comparing both models, and a summary is given.

## 2. Experiments and Analytical Methods

Single crystals of  $\{\text{N}(\text{CH}_3)_4\}_2\text{MnCl}_4$  were grown by the slow evaporation method from an aqueous solution of a stoichiometric mixture of  $\text{N}(\text{CH}_3)_4\text{Cl}$  and  $\text{MnCl}_2$  at about 300 K. A spherical specimen with a radius of 0.21 mm was prepared from a single crystal, which was light yellow, transparent, and deliquescent. The same sample as that used in our previous study was mounted on a Weissenberg-type camera installed on an imaging plate recording system (MAC SCIENCE DIP-3000). Graphite-monochromated Mo  $K\alpha$  ( $\lambda=0.07107$  nm) generated by a rotating anode at a power of 300 mA at 50 kV was used. The temperature of the specimen was controlled within  $\pm 0.1$  K using a cold nitrogen gas flow system.

In the commensurate phase III, superlattice reflections appear. The temperature dependence of the typical reflection (2 0 1/2) is shown in Fig. 3. Here, indices are referred to the normal phase I. The temperature dependence of the superlattice reflection intensity can be fitted with the power law relation

$$I(2\ 0\ 1/2) = I_0 (T_c - T)^{2\tilde{\beta}}, \quad (1)$$

where  $\tilde{\beta} = 0.363(8)$  is obtained by least-squares calculations, and the transition temperature

is estimated as  $T_c = 293$  K. The index is in agreement with the reported value.<sup>15)</sup> It should be noted that the incommensurate phase II was not found in this experiment and that the I-to-III transition took place continuously. Therefore,  $T_c$  is the I-to-III transition temperature, here. Fig. 3

X-ray diffraction intensities were collected at 292, 291, 290, 289, 287, 285, 280, 275, and 270 K (see Table II). The diffraction data were observed by the oscillating crystal method. A set of 18 photographs were taken at an oscillation angle of  $10^\circ$  and a step angle of  $10^\circ$ , indices were automatically assigned, lattice parameters were refined, and intensities were scaled between photographs.

Within phase III, the monoclinic angle  $\alpha$  stays at almost  $90^\circ$ , while the lattice parameters  $a$ ,  $b$ , and  $c$  decrease with decreasing temperature, and the reciprocal lattice parameters  $a^*$ ,  $b^*$  and  $c^*$  increase. The cell lengths and unit cell volume display kinks at  $T_c$ . The volume at 270 K shrinks by about 1.2% compared with  $T_c$ .

The space group of phase III was reconfirmed to be  $P2_1/c11$  ( $Z = 8$ ). This space group has four symmetry codes: (i)  $x, y, z$ , (ii)  $1/2-x, y, 1/2+z$ , (iii)  $1/2+x, -y, 1/2-z$ , and (iv)  $-x, -y, -z$ . Although this group is not one of the standard monoclinic groups, it is selected to set the  $a$ - and  $b$ -axes common to phase I ( $Pm\bar{c}n$ ). The diffraction intensities were collected over a wide reciprocal space, and the equivalent reflections were averaged to give more than 3,000 independent reflections. The reflections with  $F_{\text{obs}} > 5\sigma(F)$  were used for structural analysis. Here,,  $F_{\text{obs}}$  and  $\sigma(F)$  denote the observed structure factor and its estimated standard deviation, respectively. Absorption correction ( $\mu r = 0.280$ ) and Lorentz and polarization corrections were also carried out, where  $\mu$  and  $r$  denote the absorption coefficient and the radius of the specimen, respectively. Table I

The crystal data of TMatC-Mn in phase III are given in Table I at a typical temperature of 289 K. The index ranges and numbers of reflections  $N$  used in the analyses are listed in Tables I and II, respectively. Hydrogen atoms were neglected in the present analyses. Atomic scattering factors were taken from International Tables for X-ray Crystallography.<sup>21)</sup> The program AXS89 system working on a personal computer was used for the refinement of the crystal structure.<sup>22)</sup> In the block-diagonal least-squares calculations, the residual factor

$$R_w^2 = \frac{\sum_{hkl} w(hkl) \left\{ |F_{\text{obs}}(hkl)| - |F_{\text{cal}}(hkl)| \right\}^2}{\sum_{hkl} w(hkl) |F_{\text{obs}}(hkl)|^2} \quad (2)$$

was minimized with equal weight ( $w = 1$ ). Generally, the calculated structure factor  $F_{\text{cal}}$  is given by

$$F_{\text{cal}}(hkl) = \sum_j p_j \exp(-W_j) f_j \exp\left\{ 2\pi i \left[ hx_j + ky_j + lz_j \right] \right\}, \quad (3)$$

where the suffix  $j$  runs over all atoms within the unit cell, and  $f_j, x_j, y_j, z_j$ , and  $p_j$  are the atomic scattering factor, three fractional coordinates and the occupation probability of the  $j$ -th atom. The factor  $W_j$  in (3) is defined by

$$W_j = 2\pi^2 \left\{ U_{11}(ha^*)^2 + U_{22}(kb^*)^2 + U_{33}(lc^*)^2 + 2(U_{12}ha^*kb^* + U_{13}ha^*lc^* + U_{23}kb^*lc^*) \right\}. \quad (4)$$

In general,  $|F_{obs}(hkl)| \neq |F_{obs}(hk\bar{l})|$  for the monoclinic structure; however, the observed intensity symmetry looks like an orthorhombic system:  $|F_{obs}(hkl)| \cong |F_{obs}(hk\bar{l})|$ . Thus, it is considered that the real crystal consists of a number of monoclinic domains in phase III, and the observed intensity is the sum of the contribution from two kinds of domains. Therefore, we replace  $F_{cal}(hkl)$  in (2) with  $F_{ave}(hkl)$  defined as

$$|F_{ave}(hkl)|^2 = x_{dm} \cdot |F_{cal}(hkl)|^2 + (1 - x_{dm}) \cdot |F_{cal}(hk\bar{l})|^2, \quad (5)$$

where  $x_{dm}$  is the volume ratio of the monoclinic domains. In the least-squares calculations,  $x_{dm}$  was also taken as one of the fitting parameters.

In refining the crystal structure of phase III, we used two alternative models for TCM molecules: (a) order-disorder model (model A), and (b) displacive model (model B). In model A, the  $j$ -th atom can occupy two positions,  $x_j, y_j, z_j$  and  $x_j', y_j', z_j'$ , with the occupation probabilities  $p_j$  and  $p_j' = 1 - p_j$ . The atom with  $p_j > 1/2$  is called the major atom and its counterpart is called the minor atom, hereafter. The number of fitting parameters is 572. Finally, it is assumed that the occupation probabilities for atoms belonging to a tetrahedron take the same value in model A; the number of fitting parameters is 548. Table II

Firstly, the occupation probability for all the atoms including TMA was set to unity,  $p_j=1$ , in model B, and the positional parameters of each atom were refined freely. In our previous analysis at 273 K, such a model was adopted to refine the commensurate structure of phase III.<sup>19)</sup> The number of fitting parameters is 272 including the scaling factor and domain ratio. Secondly, the partially ordered TMAs were assumed, and only TCMs were treated as displacive in model B. The number of fitting parameters is 456.

The quality of the structural determinations was assessed in terms of the  $R$  factor defined by

$$R = \sum_{hkl} \left| |F_{obs}(hkl)| - |F_{ave}(hkl)| \right| / \sum_{hkl} |F_{obs}(hkl)|. \quad (6)$$

The  $R$  factors at all temperatures examined are listed in Table II for the two models. With decreasing temperature, the  $R$  factor for model B decreases as the ordering develops; however, the  $R$  factor of model A remains almost constant but lower than that of model B. This suggests

that model B is not satisfactory for describing the structure just below  $T_c$ . The significance test indicates that model B can be rejected at the 0.005 level.<sup>23)</sup> At all temperatures examined, the domain ratio parameter  $x_{dm}$  was within 0.49~0.51, almost independent of temperature for both models A and B. Therefore, the monoclinic domains were frozen in our experiment.

### 3. Structure and Temperature Variation

Essentially, the analyzed structures of phase III coincide with our previous result at 273 K.<sup>19)</sup> Taking the temperature dependences into account, we describe the difference between models A and B in the following.

Table III

Table III gives the atomic coordinates and displacement parameters at 289 K analyzed using model A (order-disorder model). The major and minor atomic parameters are given on the first and second lines, respectively. Each tetrahedral group has the same occupation probability. At the final stage of calculations, TMA(1a) and TMA(1b), and TMA(2a) and TMA(2b) were assigned the same occupation probabilities given in Table III, because the difference was small.

In Fig. 4, the crystal structure is drawn at 289 K using VESTA.<sup>24)</sup> The atomic parameters are calculated from model A, and only the major atoms are shown. In the normal phase I, the tetrahedrons labeled by (a) and (b) are related through the  $c$ -glide symmetry of  $Pm\bar{c}n$ , but they are independent in phase III. TMA(1a) and TCM(a) (and TMA(1b) and TCM(b)) construct a pseudo-hexagonal network in the  $z = 1/8$  and  $5/8$  (and  $3/8$  and  $7/8$ ) planes. Although TMA(2a) and TMA(2b) occupy the vacant space between the pseudo-hexagonal networks. Instead of the missing mirror symmetry  $1/2-x, y, z$  of phase I, the  $c$ -glide symmetry  $1/2-x, y, 1/2+z$  exists in phase III.

Fig. 4

At 289 K, the Mn-Cl bond lengths are 0.229 - 0.239 nm, the Cl-Mn-Cl angles are 103.8 - 115.4 °, the N-C bond lengths are 0.135 - 0.164 nm, and the C-N-C angles are 91.7 - 121.4 °; here, only major atoms are considered. Although the C-N-C angles show slight scattering, these lengths and angles are essentially similar to those of 273 K.<sup>19)</sup>

The atomic positions of model B almost agree with the weighted means of the major and minor atoms of model A. However, model B gives larger displacement parameters, especially for Cl atoms. For model B at 289 K, the Mn-Cl bond lengths are 0.232 - 0.237 nm, the Cl-Mn-Cl angles are 106.9 - 111.6 °, the N-C bond lengths are 0.136 - 0.164 nm, and the C-N-C angles are 90.3 - 122.5 °. The shapes of the tetrahedrons in model B are as regular as those in model A.

Now let us show the temperature variation of the structure. Figure 5 shows the temperature

dependence of  $\Delta = a(x - 1/4)$  for Mn, which represents the shift in the mass center of the TCM tetrahedron from the  $c$ -glide plane at  $x=1/4$ . Mn(a) and Mn(b) have different values because they are independent of each other in phase III. In model B, the shift  $\Delta$  increases continuously with decreasing temperature. The displacement can be fitted by

$$\Delta_j = D_j(T_c - T)^{\beta_\Delta}, \quad (7)$$

where  $\beta_\Delta = 0.52(2)$  and  $0.41(1)$  for TCM(a) and TCM(b), respectively.

Fig. 5

On the other hand, the data analyzed using model A show slight scattering, however, a small discontinuous change can be recognized in the positional parameters for the major atoms. The deviation of Mn(a) from the disordered position in phase I (shown by OD in Fig. 5)<sup>20)</sup> is opposite that of Mn(b), as if the mean positions of Mn(a) and Mn(b) are directly related to the disordered position above  $T_c$ .

Fig. 6

The temperature dependence of the rotation angles of TCM is shown in Fig. 6. The rotation axis of the tetrahedron is approximately parallel to the  $c$ -axis, and the angles  $\Theta_j$  are calculated using least-squares calculation by comparing the tetrahedron of phase III with that of the displacive model of phase I.<sup>20)</sup> These values for model A remain almost constant in phase III and coincide with those of phase I denoted by OD in Fig. 6. On the other hand, the angles change continuously in model B. The temperature dependence can be represented as

$$\Theta_j = E_j(T_c - T)^{\beta_\Theta}. \quad (8)$$

The indices are  $0.34(1)$  and  $0.31(1)$  for TCM(a) and TCM(b), respectively. Although the shifts from the  $c$ -glide plane are different between them, the temperature dependences of the rotation angle are similar to each other. As demonstrated above, the centers of mass of the TCM and TMA molecules deviate from the  $c$ -glide plane of phase III continuously, accompanying the rotation of the tetrahedral molecules. Therefore,  $\Delta_j$  and  $\Theta_j$  can be considered as order parameters of the I-to-III transition, if model B is assumed for phase III.

Next, the temperature dependence of the occupation probabilities of model A is shown in Fig. 7. As described in Table III, four kinds of occupation probabilities  $p_j$  are refined by the least-squares calculations. Each occupation probability changes similarly to the universal relation

$$p_j = 0.5 + A_j(T_c - T)^\beta, \quad (9)$$

Fig. 7

where the indices are  $0.32(3)$  and  $0.37(2)$  for TCM(a) and TCM(b), respectively. These values are almost consistent with  $\tilde{\beta} = 0.363$  of eq. (1). We can consider that the occupation probability  $p_j$  is the order parameter that describes the ordering of the commensurate phase III

in model A. All the above-mentioned power indices are summarized in Table IV, which is discussed in § 4.

Table IV

Finally, we show the temperature dependences of the atomic displacement parameters of Cl(2) in Fig. 8. These atoms have large  $U_{11}$ 's if model B is adopted. The  $U_{11}$ 's of model B increases rapidly with increasing temperature, and show a cusplike anomaly at  $T_c$ . On the other hand, the  $U_{11}$ 's of model A depend linearly on temperature and are connected continuously to the value analyzed using the disordered model in phase I.<sup>20)</sup> The temperature dependences in phases III and I will be discussed in the following section.

Fig. 8

#### 4. Discussion and Summary

The commensurate phase III of TMATC-Mn has been analyzed using both models A (order-disorder) and B (displacive) for TCM molecules. To describe the ordered structure, the split atom method is employed. In our previous report,<sup>19)</sup> the structure was analyzed at only 273 K, a sufficiently low temperature in phase III. In this report, we have refined crystal structure at nine temperatures especially in detail near  $T_c$ . The commensurately modulated structure can be described by the translations and rotations of the constituent tetrahedrons of TCM and TMA. The modulation pattern is in agreement with our previous result.<sup>19)</sup> Here, we have obtained the temperature variations in atomic positions and displacement parameters as shown in Figs. 5~8.

Firstly, we discuss the relation of structures between phases I and III. If TCM has a displacive character in the I-to-III phase transition, then phases I and III could be analyzed using the displacive (DP) model and model B, respectively. The ordering process in the commensurate phase III would be described by continuous shifts in atomic positions with temperature: the translational shifts along the  $x$ -direction and the rotations about axes within  $yz$ -planes. The determined temperature dependences are shown in Figs. 5 and 6. The continuous increases in the rotation angles  $\Theta_j$  and the positional shifts  $\Delta_j$  of TCM should be related to the temperature variation in the scattering intensity, especially the temperature dependence of the superlattice intensity shown in Fig. 3.

On the other hand, if the I-to-III phase transition has an order-disorder character, then phases I and III should be analyzed using the disordered (OD) model and model A, respectively. In phase I, tetrahedrons of TCM and TMA occupy two sites related through the mirror symmetry with equal probabilities. The occupation probability becomes unbalanced in phase III, and the mirror symmetry changes into the  $c$ -glide symmetry. As shown in Fig. 7, the ordering progresses gradually with decreasing temperature.

Secondly, let us discuss the exponents summarized in Table IV. The superlattice intensity is generally related to the square of the order parameter, that is, a spontaneous displacement from a high symmetry position or a change in the occupation probability of atom.<sup>25)</sup> As shown in Fig. 3, the superlattice reflection increases its intensity monotonically with decreasing temperature, which indicates the critical index  $\tilde{\beta}$  to be 0.363. Such a nonclassical exponent is often observed in the normal-incommensurate transition in  $A_2BX_4$ -type compounds, that is, the phase transition is of either the order-disorder or displacive type.<sup>8, 11)</sup> It is well known that such an index is understood if the system is described by a  $3d-xy$  model Hamiltonian. Here, the  $xy$  model means that the number of the critical degrees of freedom is two; one is the amplitude and the other is the phase of a one-dimensional modulation wave that characterizes the modulation structure.<sup>12)</sup> In §3, we have presented several quantities as candidates for the order parameter:  $\Delta_j$ ,  $\Theta_j$ , and  $p_j$ , which are given in Table IV. The indices  $\beta$  for the occupation probability of model A are almost in agreement with  $\tilde{\beta}$ . The index  $\beta_\circ$  for model B is in good agreement with  $\tilde{\beta}$ , and  $\beta_\Delta$  is not.

Thirdly let us consider the atomic displacement parameters, which are often treated as thermal parameters. Imagine that a distribution of atom is represented by two peaks at the positions of  $x_1$  and  $x_2$ . The probability to find the atom at an interval of  $\Delta x$  will be written as

$$P(x)\Delta x = \{pf(x-x_1) + (1-p)f(x-x_2)\}\Delta x. \quad (10)$$

Here, the function  $f(x)$  is normalized and symmetric  $f(x)=f(-x)$ . The parameter  $p$  represents the peak ratio with  $0 \leq p \leq 1$ . Such an example has already been shown in Fig. 2. The expectation values are easily calculated as

$$\langle x \rangle = \int xP(x)dx = px_1 + (1-p)x_2 = \bar{x} + (2p-1)d, \quad (11)$$

$$\langle (x - \langle x \rangle)^2 \rangle = \int x^2 f(x)dx + px_1^2 + (1-p)x_2^2 - \langle x \rangle^2 = \sigma + 4p(1-p)d^2, \quad (12)$$

where  $\bar{x} = (x_1 + x_2)/2$  and  $d = (x_1 - x_2)/2$ . The second moment of the function  $f(x)$  is represented by the variance  $\sigma$ . If the atom is within a harmonic potential  $V(x) = cx^2/2$ , as assumed by Itoh,<sup>26)</sup> then  $\sigma = k_B T/c$  is the variance of the Gaussian distribution. Here,  $k_B$  is Boltzmann's constant. Furthermore, we can introduce the order parameter  $S$  as  $S = 2p - 1$  in the case of order-disorder transitions. Then eq. (12) is identical to eq. (8) in ref. 26.

Here, we note that eqs. (11) and (12) are employed to draw an equivalent Gaussian distribution (PG) denoted by the open circles in Fig. 2. The parameters are  $x_1 = d = 0.6$ ,

$x_2 = -d$ ,  $\sigma = 0.5$ , and (a)  $p = 0.5$  and (b)  $p = 0.7$  in Fig. 2.

Let us comment on  $f(x)$ : (i) The atomic displacement parameter  $U_{11}$  in eq. (3) is the second moment eq. (12) along the  $x$ -axis, if the function  $f(x)$  is Gaussian. Since the structure factor eq. (3) is the Fourier transform of the electron density in the unit cell, the factor  $\exp(-W_j)$  in eq. (3) is the Fourier transform of the density distribution of the nuclei. When  $P(x)$  takes a Gaussian form, the Fourier transformed form is given by (3). (ii) The potential  $V(x)$  is not necessarily a harmonic function, and the transition is not of order-disorder type. Let us imagine that an atom is moving within an anharmonic potential and the square of the wavefunction of nuclei can be approximately represented by eq. (10). Even in such a displacive case, we obtain eqs. (11) and (12), but  $p$  is just a parameter for representing  $P(x)$ .

The high-symmetry phase is represented by  $p = 1/2$ , so that  $\langle x \rangle = \bar{x}$  and the temperature parameter of the atom  $U_{\text{HT}}$  is given by

$$U_{\text{HT}} = \left\langle (x - \langle x \rangle)^2 \right\rangle = \sigma + d^2 . \quad (13)$$

In the low-symmetry phase, the atomic displacement parameter of the atom is given by eq. (12). For an ideal order-disorder system, the splitting parameter  $d$  may be constant and only the occupation probability  $p$  changes with temperature. We can estimate  $\sigma$  from the atomic displacement parameter of the split atom and  $p$  from the occupation probability, by analyzing model A for the disordered phase. On the other hand,  $d$  is considered zero in an ideal displacive case, and the temperature variation in  $\sigma$  (caused by the symmetry change of phase transition) may give some characteristic behavior of the atomic displacement parameter at approximately  $T_c$ .<sup>27)</sup>

The atomic displacement parameters for  $U_{11}$  of Cl(2) are shown in Fig. 8. If model A is adopted, the atomic displacement parameter simply shows a monotonic change through the transition; the parameter is proportional to temperature. Thus, the order-disorder model can explain the temperature dependence of the atomic displacement parameters naturally. However, the displacive model for Cl(2) in phase I indicates a maximum at  $T_c$ , below which  $U_{11}$  drops and approaches that of model A. In particular,  $U_{11}$  increases slightly with decreasing temperature in phase I; it also shows a sharp maximum at  $T_c$ . It has been argued sometimes that such behavior stems from the critical fluctuation in the displacive nature of the transition.<sup>28)</sup> However, the atomic displacement parameter represents only the mean square vibration of atoms in a single-particle potential. We consider that the split distance of Cl(2) increases as the short-range order develops near  $T_c$ ,<sup>20)</sup> so it is irrelevant to the critical behavior

of the pair correlation function at the transition point. Equation (13) explains the overall atomic displacement parameter determined using the displacive model in phase I. Therefore, the order-disorder structure model is most appropriate. The cusplike maximum of  $U_{11}$  for Cl(2) may stem from inadequacy of displacive model analysis.

We summarize our results again. In our previous study,<sup>20)</sup> the crystal structure of the normal phase I was investigated in detail. We concluded that two kinds of TMA are disordered, while TCM (especially its translational degree of freedom) may be disordered or displacive. Although the difference between the two models was not large, we can conclude now that the disordered model is appropriate for the normal structure of phase I, because model A is also reasonable in determining the temperature dependence of the atomic displacement parameters.

Finally, we comment on model A. The transition at  $T_c$  seems to be continuous; however, the atomic position of Mn seems to be discontinuous, as shown in Fig. 5, if model A is adopted. At first glance, these seem to be inconsistent. However, the shift  $\Delta$  in Fig. 5 for model A indicates the peak position of the major atomic density. In actually, a minor atomic density exists in addition to a major one, although both positions are rather close to each other. If the total atomic density is considered as in eq. (10), the weighted mean position  $\langle x \rangle$  changes continuously with decreasing temperature. In the case of TMA, two sites are largely separated, so that the atomic density of the minor part decreases, while that of the major part increases rapidly. On the other hand, the major and minor parts of Mn and Cl are not highly separated, so that the total atomic distribution is single and asymmetric. As the minor part disappears, the peak position of the distribution shifts and becomes continuously symmetric, as if the ordering of TCM is displacive; the continuous character of the phase transition is ensured. The detailed analysis was discussed on the basis of Fourier maps reported elsewhere.<sup>29)</sup>

The order-disorder character (i.e. atoms can be represented successfully by split ones) of the normal phase is similar to that of the isomorphous crystal of TMAZC-Zn.<sup>18)</sup> Specific heat measurement gave a transition entropy almost as large as  $R \ln 4$ , which supports the order-disorder nature of the transition in TMAZC-Mn.<sup>30)</sup> However, the transition character is not considered literally. The ordering of the disordered structure may accompany continuous positional shifts in a manner discussed as above.

## Acknowledgments

One of the authors (NK) thanks Dr. H. Kasano and Mr. T. Miyoshi for encouraging

discussions throughout this work. The data collection was performed using the Weissenberg camera (DIP3000) at the Center of Instrumental Analysis, Yamaguchi University.

- 1) S. Sawada, Y. Shiroishi, A. Yamamoto, M. Takashige, and M. Matsuno: J. Phys. Soc. Jpn. **44** (1978) 687.
- 2) S. Sawada, Y. Shiroishi, A. Yamamoto, M. Takashige, and M. Matsuno: Phys. Lett. A **67** (1978) 56.
- 3) M. Iizumi, J. D. Axe, G. Shirane, and K. Shimaoka: Phys. Rev. B **15** (1977) 4392.
- 4) H. Shimizu, N. Abe, N. Yasuda, S. Fujimoto, S. Sawada, and Y. Shiroishi: Jpn. J. Appl. Phys. **18** (1979) 857.
- 5) H. Shimizu, A. Oguri, N. Abe, N. Yasuda, S. Fujimoto, S. Sawada, Y. Shiroishi, and M. Takashige: Solid State Commun. **29** (1979) 125.
- 6) H. Shimizu, N. Abe, N. Kokubo, N. Yasuda, S. Fujimoto, T. Yamaguchi, and S. Sawada: Solid State Commun. **34** (1980) 363.
- 7) K. Gesi and K. Ozawa: J. Phys. Soc. Jpn. **53** (1984) 627.
- 8) J. D. Axe, M. Iizumi, and G. Shirane: *Incommensurate Phases in Dielectrics 2. Materials* (North-Holland, Amsterdam, 1986) Chap. 10, p. 1.
- 9) N. Hamaya, Y. Fujii, S. Shimomura, Y. Kuroiwa, S. Sasaki, and T. Matsushita: Solid State Commun. **67** (1988) 329.
- 10) S. Shimomura, N. Hamaya, and Y. Fujii: Phys. Rev. B **53** (1996) 8975.
- 11) H. Mashiyama: J. Phys. Soc. Jpn. **50** (1981) 2655.
- 12) A. D. Bruce and R. A. Cowley: *Structural Phase Transitions*, (Taylor and Francis, 1981, London), Chap. 1 and 2.
- 13) H. Mashiyama: J. Korean Phys. Soc. **29** (1996) S419.
- 14) R. Blinc, M. Burgar, J. Slak, V. Rutar, and F. Milia: Phys. Status Solidi A **56** (1979) K65.
- 15) H. Mashiyama and S. Tanisaki: J. Phys. Soc. Jpn. **50** (1981) 1413.
- 16) H. Mashiyama S. Tanisaki, and K. Gesi: J. Phys. Soc. Jpn. **50** (1981) 1415.
- 17) H. Mashiyama and S. Tanisaki: J. Phys. C: Solid State Phys. **15** (1982) L455.
- 18) K. Hasebe, H. Mashiyama, N. Koshiji, and S. Tanisaki: J. Phys. Soc. Jpn. **56** (1987) 3543.
- 19) H. Mashiyama and N. Koshiji: Acta Cryst. B **45** (1989) 467.
- 20) N. Koshiji and H. Mashiyama: J. Phys. Soc. Jpn. **69** (2000) 3853.
- 21) IUCr: *International Tables for X-ray Crystallography*, (Kluwer Academic Pub. 1999, London) C, 548.
- 22) H. Mashiyama: J. Phys. Soc. Jpn. **60** (1991) 180.
- 23) W. C. Hamilton: Acta Cryst. **18** (1965) 502.
- 24) K. Momma and F. Iizumi: J. Appl. Crystallogr. **41** (2008) 653.
- 25) T. Mitsui, I. Tatsuzaki, and E. Nakamura: *An Introduction to the Physics of Ferroelectrics*, (Gordon and Breach, 1976, London), Chap. 5.
- 26) K. Itoh: J. Phys. Soc. Jpn. **53** (1984) 2049.
- 27) H. Mashiyama, M. Ashida, and S. E. Mkam Tchouobiap: Meet. Abstr. Phys. Soc. Jpn. **63** (2008) Issue 2, 877.

- 28) K. Itoh: J. Crystallogr. Soc. Jpn. **28** (1986) 247 [in Japanese] .  
 29) N. Koshiji and H. Mashiyama: presented at the 8th Japan-Korea Conf. on Ferroelectrics, 2010.  
 30) J. Zubillaga, A. Lopez-Echarri, and M. J. Tello: J. Phys. C: Solid State Phys. **21** (1988) 4417.

Table I. Crystal data of  $\{\text{N}(\text{CH}_3)_4\}_2\text{MnCl}_4$  at 289 K in phase III.

Space group	$P2_1/c11$
$Z$	8
$a$ (nm)	0.9057
$b$ (nm)	1.5642
$c$ (nm)	2.4723
$\alpha$ ( $^\circ$ )	90.054
Index range	$0 \leq h \leq 11$ $0 \leq k \leq 21$ $-34 \leq l \leq 34$

Table II.  $R$  factors for models A and B. The measured temperatures and numbers of reflections  $N$  are shown.

Temperature (K)	$N$	model A	model B
292	3013	0.0746	0.0802
291	3206	0.0745	0.0806
290	3335	0.0745	0.0791
289	3456	0.0729	0.0791
287	3595	0.0719	0.0774
285	3664	0.0714	0.0767
280	3880	0.0730	0.0785
275	3991	0.0669	0.0759
270	4105	0.0700	0.0773

Table III. Atomic coordinates, equivalent isotropic displacement parameters ( $\text{pm}^2$ ), and occupation probabilities for model A at 289K in phase III with e.s.d.'s in parentheses. The second line gives the minor atom parameters.

Group	Atom	$x$	$y$	$z$	$U$	$p$
TCM(a)	Mn (a)	0.2525 (3)	0.4061 (2)	0.1209 (1)	481 (7)	0.776 (4)
		0.2496 (9)	0.4165 (6)	0.1306 (3)	500(27)	0.224
	Cl (1a)	0.2666 (6)	0.4083 (5)	0.0285 (2)	860 (22)	
		0.2203 (21)	0.4055 (17)	0.0317 (7)	883 (79)	
	Cl (2a)	0.2853 (7)	0.5458 (5)	0.1582 (3)	994 (26)	
		0.2197 (23)	0.5493 (17)	0.1505 (10)	1020 (91)	
	Cl (3a)	0.0245 (6)	0.3478 (5)	0.1502 (2)	1018 (28)	
		0.0506 (22)	0.3450 (15)	0.1649 (9)	1053( 84)	
	Cl (4a)	0.4457 (6)	0.3282 (5)	0.1572 (3)	1049 (26)	
		0.4711 (19)	0.3279 (17)	0.1490 (8)	982 (94)	
TCM(b)	Mn (b)	0.2659 (3)	0.0922 (2)	0.3723 (1)	485 (7)	0.750 (4)
		0.2394 (8)	0.0973 (6)	0.3757 (3)	485 (22)	0.250
	Cl (1b)	0.2582 (7)	0.1009 (5)	0.2770 (2)	956 (25)	
		0.2594 (22)	0.0710 (15)	0.2779 (6)	972 (81)	
	Cl (2b)	0.2966 (7)	-0.0462 (5)	0.4077 (3)	967 (25)	
		0.2299 (21)	-0.0449 (13)	0.4089 (7)	922 (69)	
	Cl (3b)	0.0355 (6)	0.1452 (5)	0.4046 (3)	1027 (29)	
		0.0610 (18)	0.1821 (15)	0.4039 (8)	1034 (75)	
	Cl (4b)	0.4605 (6)	0.1802 (5)	0.4020 (3)	957 (24)	
		0.4709 (20)	0.1413 (17)	0.4035 (8)	1121 (97)	
TMA(1a)	N (1a)	0.2608 (14)	0.0929 (12)	0.0748 (7)	816 (64)	0.793 (20)
		0.2366 (51)	0.0935 (41)	0.0667 (17)	678 (178)	0.207
	C (1a)	0.2474 (32)	0.1023 (16)	0.1347 (6)	1069 (102)	
		0.2564 (77)	0.0783 (44)	0.1435 (20)	604 (206)	
	C (2a)	0.2209 (28)	0.0076 (15)	0.0507 (7)	993 (90)	
		0.2967 (88)	0.0093 (52)	0.0487 (24)	875 (276)	
	C (3a)	0.1648 (32)	0.1595 (19)	0.0449 (10)	1416 (126)	
		0.1180 (112)	0.1099 (109)	0.0435 (38)	1753 (744)	
	C (4a)	0.4057 (26)	0.1181 (25)	0.0535 (10)	1826 (165)	
		0.2939 (87)	0.1722 (63)	0.0379 (26)	1120 (332)	
TMA(1b)	N (1b)	0.2541 (14)	0.4021 (9)	0.3241 (4)	479 (40)	0.793
		0.2452 (57)	0.3952 (37)	0.3324 (22)	658 (193)	0.207
	C (1b)	0.2551 (32)	0.3819 (25)	0.3780 (9)	1616 (166)	
		0.2582 (95)	0.2519 (63)	0.3739 (34)	926 (360)	
	C (2b)	0.2204 (33)	0.4927 (17)	0.3160 (8)	1341 (112)	
		0.2975 (184)	0.4521 (139)	0.3225 (37)	2980 (1118)	
	C (3b)	0.1545 (33)	0.3374 (21)	0.3080 (10)	1611 (140)	
		0.1344 (90)	0.3839 (57)	0.3533 (43)	1844 (355)	
	C (4b)	0.4058 (24)	0.3818 (23)	0.3166 (11)	1458 (145)	
		0.2695 (90)	0.2918 (84)	0.3058 (30)	2059 (474)	
TMA(2a)	N (2a)	0.7573 (16)	0.3293 (10)	0.0078 (5)	512 (49)	0.718 (19)
		0.7390 (36)	0.3292 (22)	0.0101 (14)	467 (108)	0.282
	C (5a)	0.7750 (32)	0.2385 (18)	0.0315 (12)	1194 (117)	
		0.7219 (71)	0.2406 (44)	0.0331 (28)	1157 (264)	
	C (6a)	0.6746 (29)	0.3792 (22)	0.0405 (11)	1445 (125)	
		0.8182 (55)	0.3784 (40)	0.0427 (21)	1116 (196)	
	C (7a)	0.6893 (37)	0.3201 (22)	-0.0536 (11)	1665 (142)	
		0.5818 (42)	0.3524 (37)	0.0002 (23)	765 (194)	
	C (8a)	0.9065 (23)	0.3617 (18)	-0.0006(11)	1011 (105)	
		0.8176 (74)	0.3315 (43)	-0.0526 (19)	1486 (236)	
TMA(2b)	N (2b)	0.7588 (16)	0.1783 (11)	0.2511 (7)	640 (59)	0.718
		0.7439 (41)	0.1840 (33)	0.2477 (12)	756 (164)	0.282
	C (5b)	0.7621 (30)	0.2674 (19)	0.2692 (13)	1258 (122)	
		0.7323 (54)	0.2707 (36)	0.2585 (20)	744 (177)	
	C (6b)	0.7455 (38)	0.1054 (23)	0.2918 (10)	1383 (143)	
		0.7684 (128)	0.0819 (68)	0.2454 (36)	1890 (548)	
	C (7b)	0.6268 (26)	0.1560 (23)	0.2268 (12)	1393 (151)	
		0.6804 (110)	0.1033 (77)	0.2258 (25)	2216 (535)	
	C (8b)	0.8936 (30)	0.1452 (24)	0.2290 (13)	1456 (174)	
		0.8556 (89)	0.1734 (51)	0.2269 (32)	1390 (350)	

Table IV. Four kinds of power indices with e.s.d.'s in parentheses.

	Index	Molecule	Value
Integrated Intensity	$\tilde{\beta}$		0.363(8)
model A	$\beta$	TCM(a)	0.32(3)
	$\beta$	TCM(b)	0.37(2)
	$\beta$	TMA(1a,1b)	0.31(1)
	$\beta$	TMA(2a,2b)	0.44(1)
model B	$\beta_{\Delta}$	TCM(a)	0.52(2)
	$\beta_{\Delta}$	TCM(b)	0.41(1)
	$\beta_{\ominus}$	TCM(a)	0.34(1)
	$\beta_{\ominus}$	TCM(b)	0.31(1)

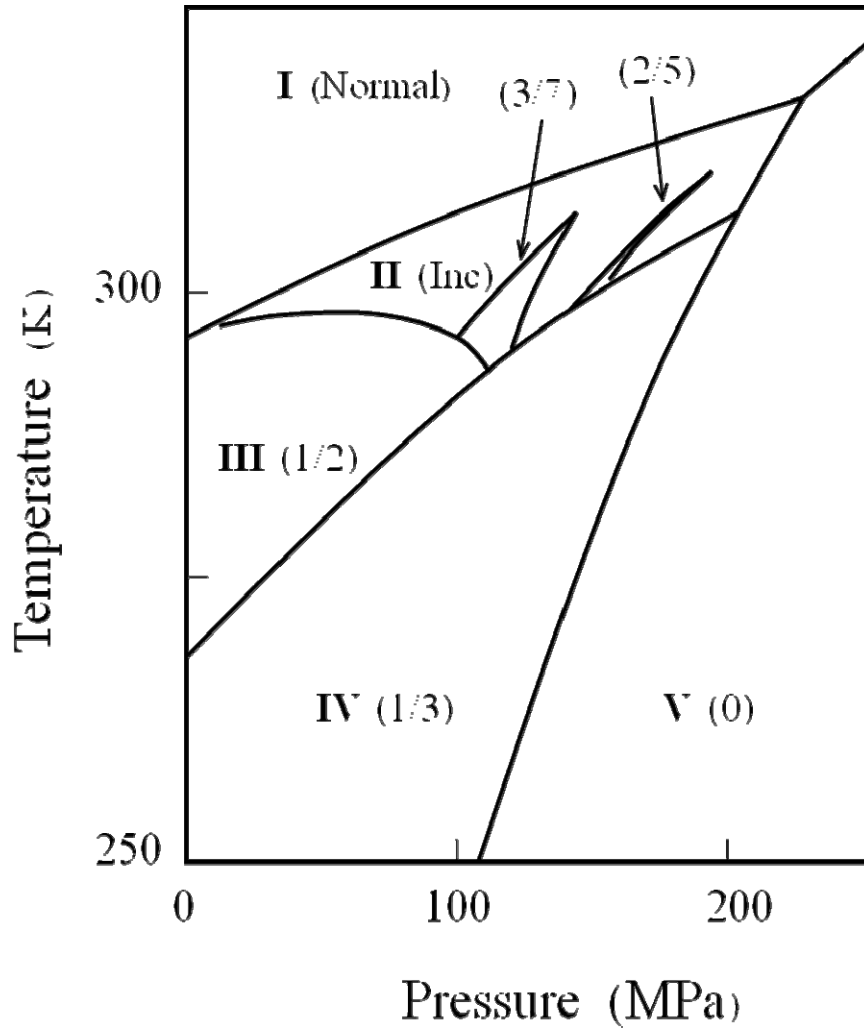


Fig. 1. Schematic  $p$ - $T$  phase diagram of TMATC-Mn. A number of commensurate phases are found under pressure. The reduced wave number of the modulated phase is indicated in parentheses.

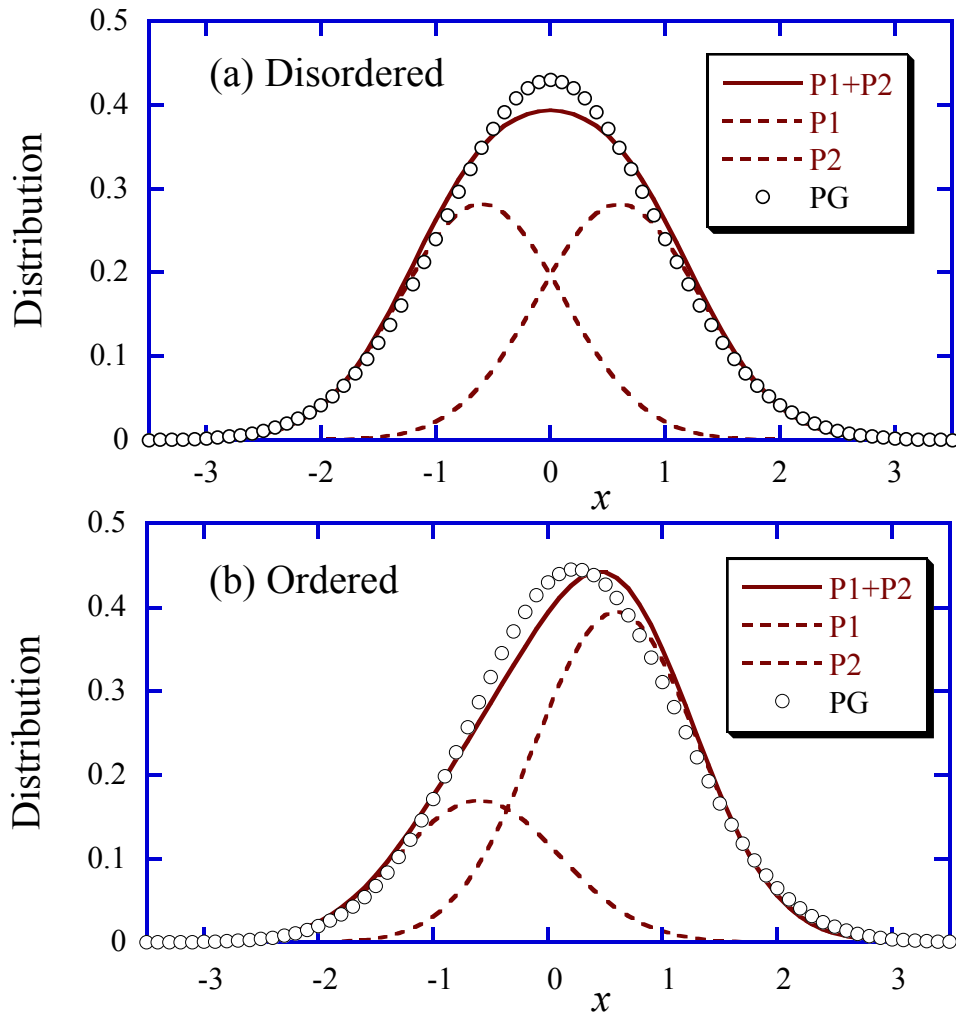


Fig. 2. (color online) Schematic atomic distributions of (a) disordered state and (b) ordered state. The total distribution is composed of two Gaussian functions, P1 and P2, located at  $x = \pm 0.6$ , respectively, whose variance is 0.5. The summation P1+P2 may be well fitted to a single Gaussian distribution (PG) denoted by open circles. The ratio P1:P2 is 5:5 in (a) and 7:3 in (b).

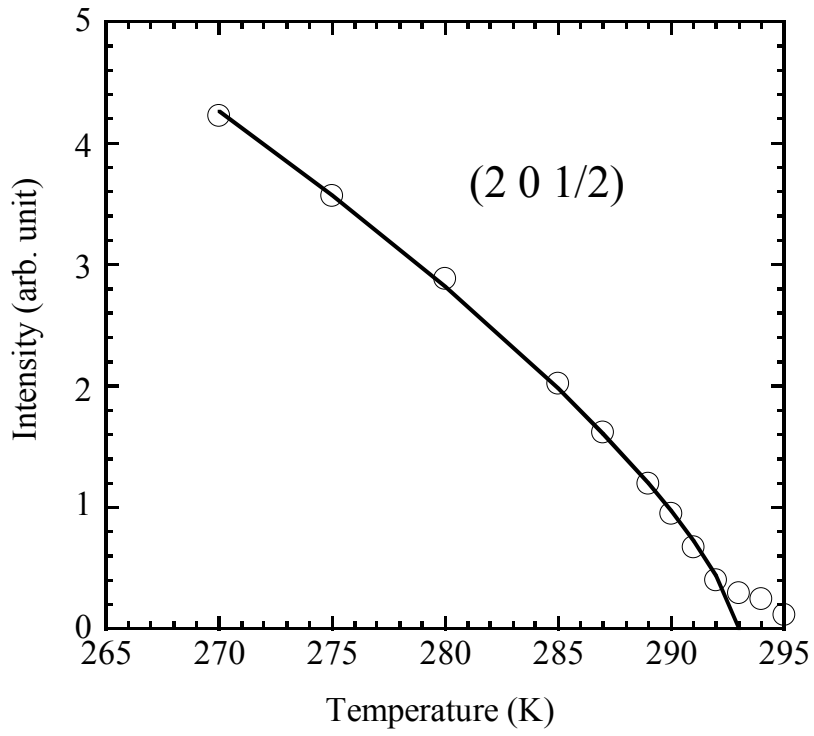


Fig. 3. Temperature dependence of the superlattice intensity (2 0 1/2), where indices are referred to those in phase I. The intensity obeys  $I \propto (T_c - T)^{2\tilde{\beta}}$ , where  $\tilde{\beta} = 0.363$ . At approximately  $T_c = 293$  K, diffuse scattering intensities are recognized.

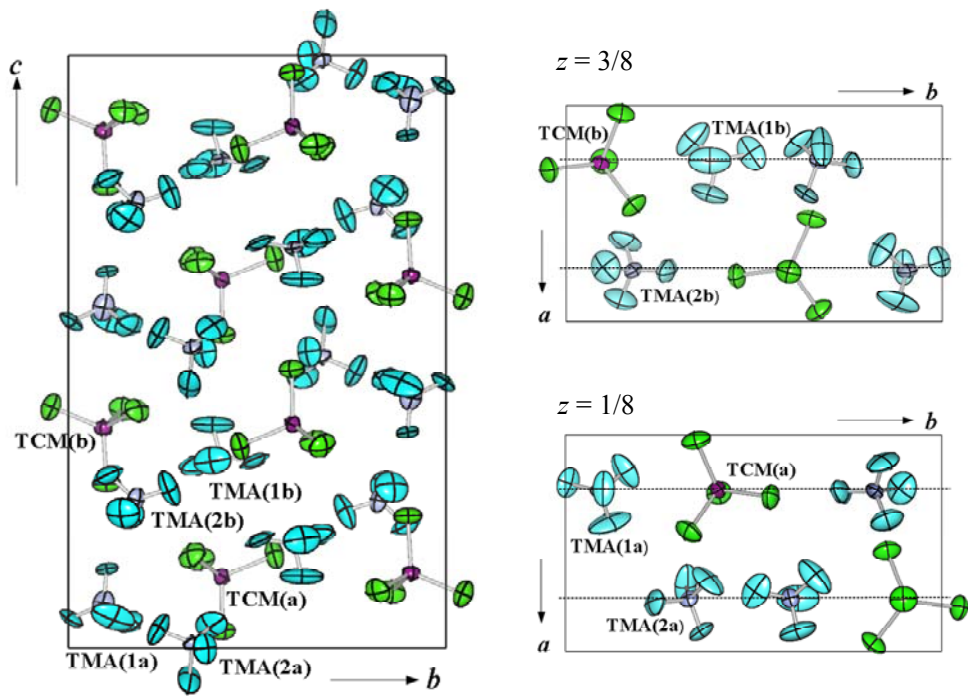


Fig. 4. (color online) Schematic pictures of the commensurate phase III of TMATC-Mn at 289 K for model A. Only major atomic positions are drawn. The left figure shows the  $a$ -axis projection. The right figures are projected on the  $ab$ -plane; the top and bottom show the layers around  $z \cong 3/8$  and  $1/8$ , respectively. The dot lines indicate  $c$ -glide planes at  $x = 1/4$  and  $3/4$ . Ellipsoids represent the atomic displacement parameters.

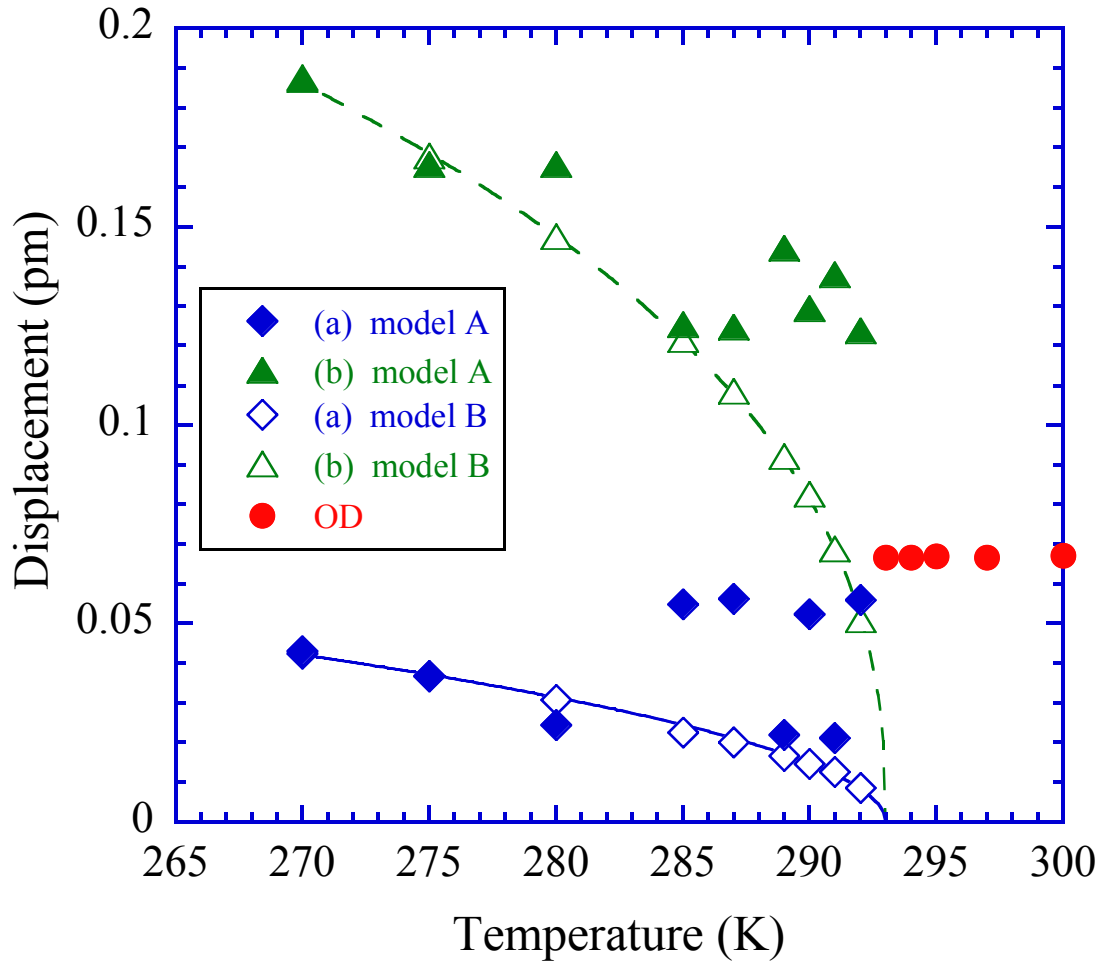


Fig. 5. (color online) Temperature dependence of the shift of Mn from the  $c$ -glide plane. For model A, the shift of Mn(b) is larger than that of phase I (closed circles denoted by OD). The shift of Mn(a) is so small that the data are scattered a little. The solid and broken curves indicate the relations fitted to eq. (7) for model B. The displacement of OD is taken from the disordered model given in ref. 20.

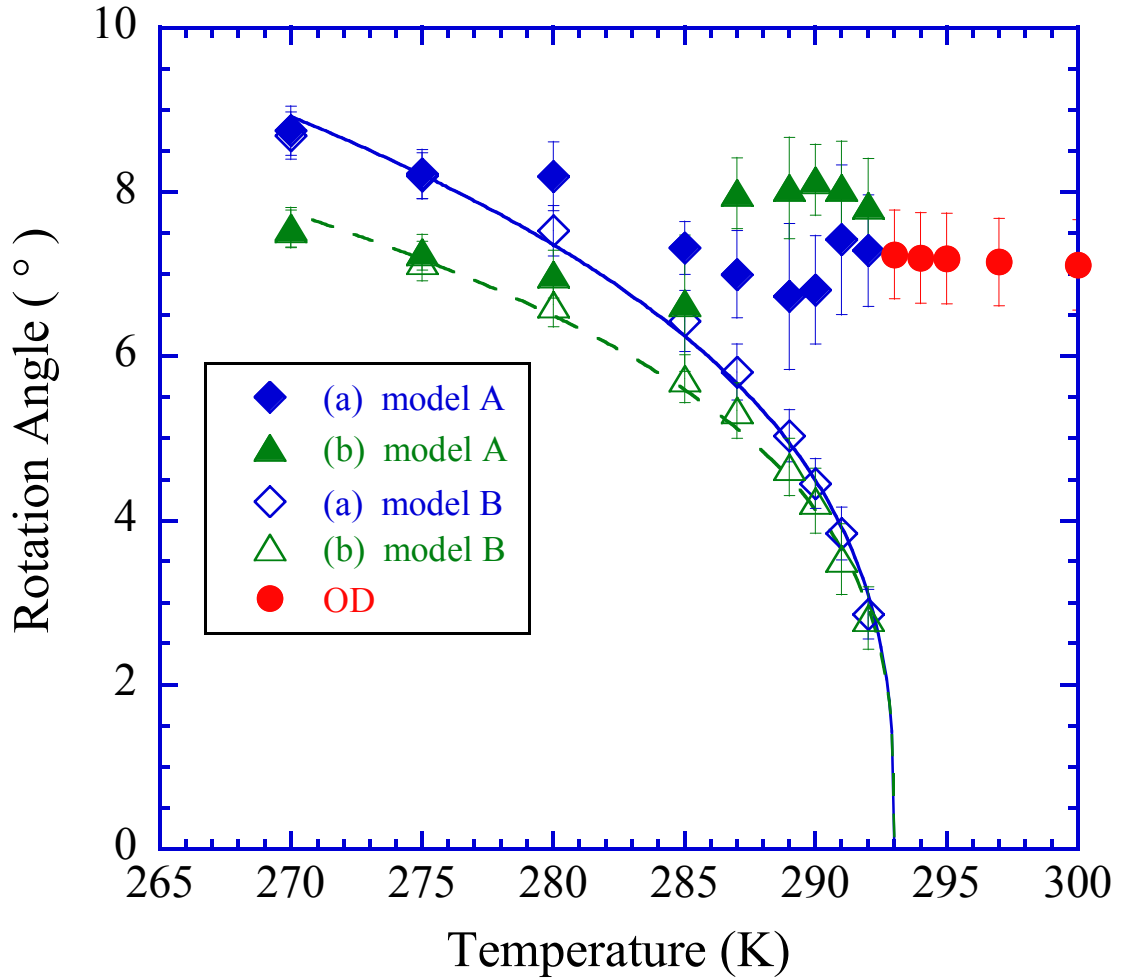


Fig. 6. (color online) Temperature dependences of the rotation angles of TCM(a) and TCM(b). For model A, both (a) and (b) are almost temperature-independent and maintain the angle of phase I, as indicated by the closed circles (OD). The solid and broken curves indicate the relation fitted to eq. (8) for model B; both (a) and (b) increase continuously with decreasing temperature. The rotation angle of OD is taken from the disordered model given in ref. 20.

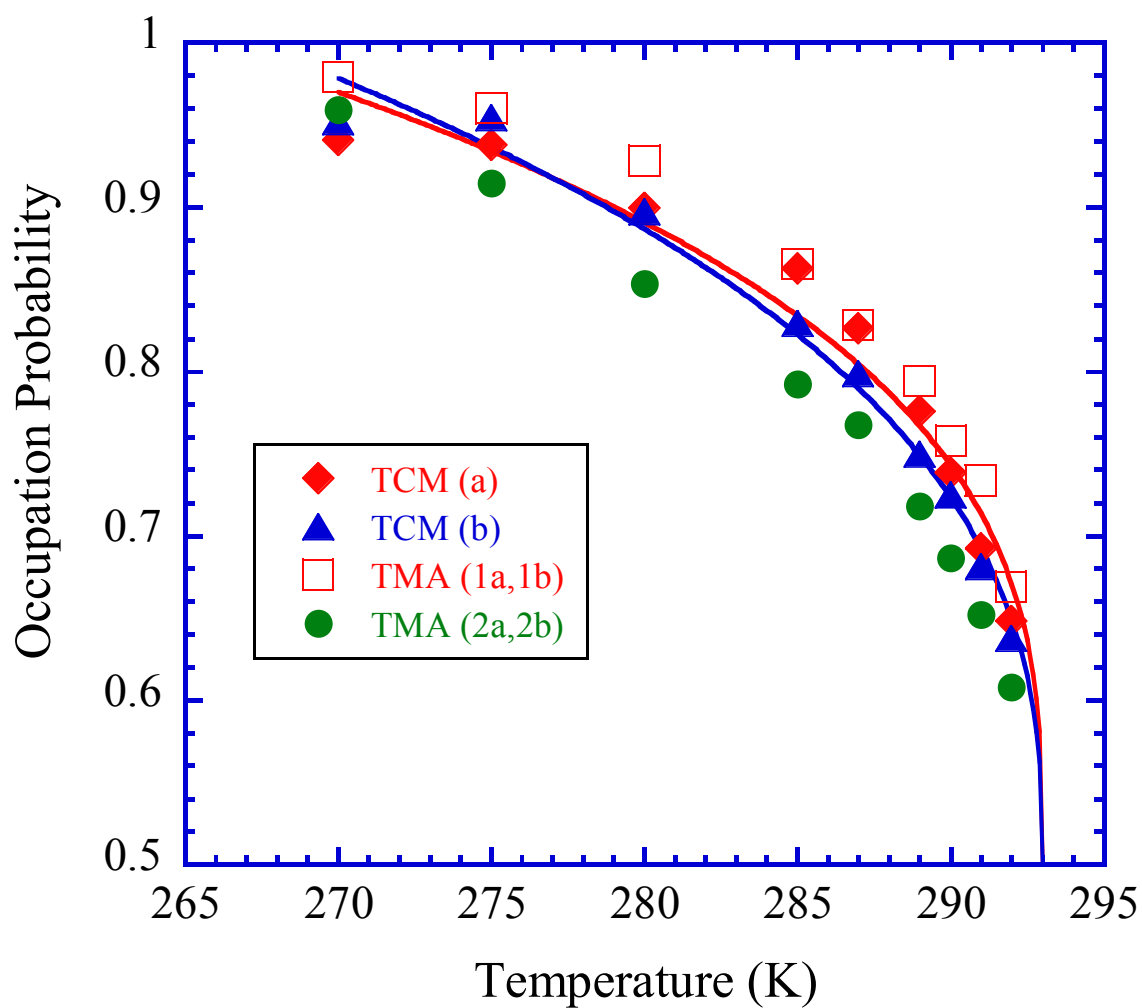


Fig. 7. (color online) Temperature dependences of the occupation probability of tetrahedral molecules. The solid curves are the fitted relation  $p_j \sim (T_c - T)^\beta$ , where  $\beta=0.32$  and  $0.37$  for TCM(a) and TCM(b), respectively. The occupation probabilities of TMA are also plotted without a fitting curve.

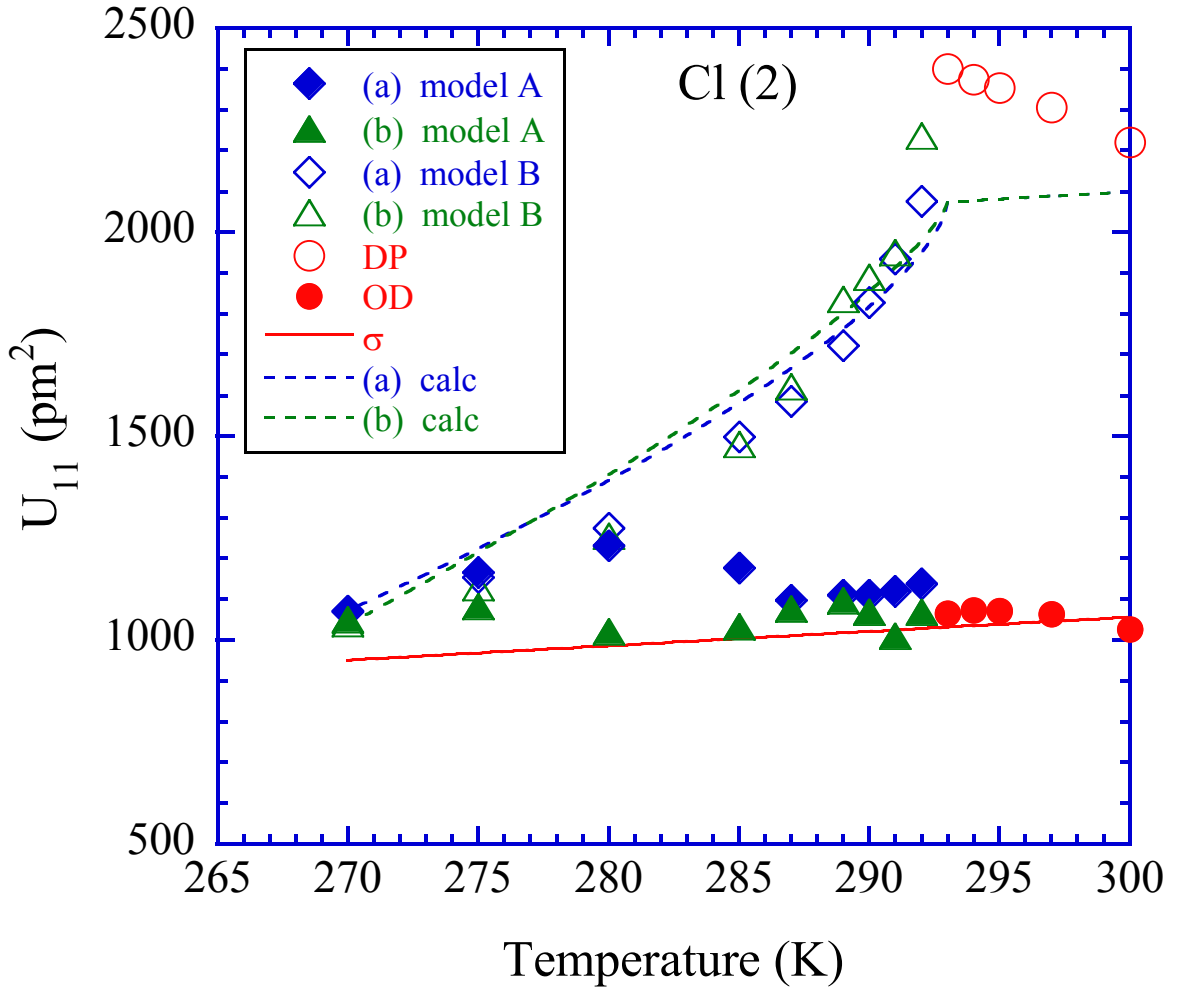


Fig. 8. (color online) Temperature dependence of the atomic displacement parameter  $U_{11}$  of Cl(2). The solid line ( $\sigma$ ) indicates the linear dependence of  $U_{11}$  on temperature, which is a good guide for model A and for the disordered model of phase I (closed circles denoted by OD). If model B (phase III) and the displacive model of phase I (open circles denoted by DP) are adopted,  $U_{11}$  shows a cusp at  $T_c$ . The calculated eq. (13) is shown by the broken lines. The symbols denoted by DP and OD are taken from the displacive and disordered models given in ref. 20, respectively.